A Human (Clovis)/Gomphothere (*Cuvieronius*) Association ~13,390 cal years B.P in Sonora, Mexico

SUPPORTING INFORMATION

Vance T, Holliday, Andrew Kowler, Todd Lange, Susan M. Mentzer, Gregory Hodgins, Natalia Martínez-Tagüeña, Edmond P. Gaines, Joaquin Arroyo-Cabrales, Guadalupe Sanchez, Ismael Sanchez

Excavation Procedures

A metric grid system was established to maintain horizontal control of the excavation . In order to facilitate excavation, the grid was established at the same orientation as the Locality 1 topographic island at 329.3° (i.e., 30.7 degrees west of north) (Fig. S1) Excavation units are referenced to the metric grid system, thus providing horizontal control over all excavation areas. Using this scheme, *in situ* artifacts recovered during the course of investigation were plotted horizontally with sub-centimeter precision in reference to northing (N) and easting (E) coordinates.

Each 1x1m unit was excavated in 50x50 cm squares and in 5cm levels or to the top of the next stratigraphic break; whichever was encountered first. All material recovered on the screens, therefore, could be given a provenience to within 50x50 cm and $\leq$ 5cm depth. In the 2008 season, most of the excavated matrix was water screened, but this was discontinued in subsequent seasons owing to logistical difficulties in getting water to the site. By the end of excavations in the last (2011-2012) season all of Locality 1 was excavated into upper stratum 3B from the E160 line eastward to the east tip of the island. Two test units were excavated at the west end of the island down to stratum 3B (Fig. S1). No bone was recovered in these units, indicating that the excavations east of E160 recovered most if not all of the remaining upper bone bed.

Site Stratigraphy and Formation Processes

Geoarchaeological analyses, which included field-based geomorphology and sedimentary description, laboratory analyses of loose sediment samples, and micromorphology reveal that the alluvial and palustrine sediments in the investigated localities were deposited in a series of ancient channels and basins. Subsequent erosion produced an inverted landscape. The stratigraphic isolation of Locality 1 thus makes paleotopographic reconstruction impossible. Only very broad parameters of the strata 3 and 4 basins can be established based on the presence of stratum 2 and older deposits, and absence of strata 3 and 4 in all neighboring exposures (text Fig. 2). From Locality 1 northwest to the nearest stratum 2 outcrop is ~75m, and from Locality 1 southwest to the nearest stratum 2 exposure is ~25m. The stratum 3 channel and the stratum 4 basin, therefore, could be no more than 100m wide. Exposures of stratum 4 from Locality 1 southeast to a remnant of stratum 4 where point #46023 was found (Fig. S1) provides a minimum width of 32m for the stratum 4 basin.

The stratigraphy along the eastern end of Locality 1 is generally uniform on both the north and south walls from E148 to E160 (Table S1) (i.e., the area of excavation of the intact upper bone bed) (text Fig. 3). The field description below is typical of the excavation area. East from about the E160 line to the east tip of the island the stratigraphy is strongly mixed by bioturbation (Fig. S1), as indicated by krotovinas 10-50 cm in diameter. This bioturbation caused local collapse of the stratigraphic section (Fig. S5). The zone of diatomite at the base of stratum 4 thins to the west as the top of stratum 3 gently rises to the west. Throughout most of the excavation area the zone of pure diatomite is 8-10cm thick. Along the E148 wall it is generally 8cm thick. The diatomite pinches out at ~E146 (Fig. S5). At E134 in the 1x4 m test unit near the north wall (Fig. S1) stratum 4 is 65cm thick. Just east at E128/N534 in the 2x2 test stratum 4 is 60cm thick (Fig. S1).

The laboratory analyses of the Locality 1 sediments included particle size, and measurements of total organic carbon and abundance of calcium carbonate (results not reported here). Micromorphological analyses were conducted on oriented sediment blocks that were

collected from the excavation profiles. The entire stratigraphic sequence was sampled in order to obtain a permanent record of the site. At the University of Arizona, the blocks were oven-dried and impregnated with a mixture of polyester resin diluted with styrene and catalyzed with methyl ethyl ketone peroxide. The hardened blocks were sliced with a rock saw, and selected portions of the sequence were father processed by trimming to 5 x 7 cm tiles. The tiles were mounted on glass slides and ground to a thickness of 30 micros by Quality Thin Sections (Tucson, AZ). The thin sections were studied at a variety of magnifications and under different types of light using stereomicroscopes and petrographic microscopes equipped with plane polarized light, cross-polarized light, darkfield illumination, and fluorescence. Micromorphological analyses were conducted at the University of Arizona and the University of Tuebingen, following standardized criteria for general descriptions (*1*) and microscopic features of carbonate samples (*2,3*).

The microscopic characteristics of the top of stratum 3 and the entirety of stratum 4 in Locality 1 are indicative of progressive development and evolution of a wetland environment (Fig. S3). At a microscopic scale, the contact between the two strata is abrupt. The poorly sorted coarse, dominantly igneous sands of stratum 3 (but including sand-sized fragments of bone) are overlain by several millimeters of finer sediment containing fine sand- and silt-sized materials. The fine sediments are in turn overlain by a nearly pure diatomite exhibiting strong laminations, horizontally aligned, intact diatoms, and thin lenses of fine sand, all faintly visible in the field (Table S1). The lack of fragmentation of the diatoms indicates that water energies were low, in keeping with its lacustrine character. The two strata differ markedly in porosity. Stratum 3 contains abundant channels and cracks, while stratum 4 is massive and contains few voids. Bioturbation features are visible in thin section, including mm-scale insect burrows that cross-cut the stratigraphic contact and contribute to upward movement of stratum 3 material into stratum 4. Above the layer of pure diatomite that comprises the base of stratum 4, the diatomaceous earth is characterized at micro-scale by sediment rich in diatoms, but also containing lenses of degraded organic material and phytoliths, and lenses of fine sand. Weakly expressed bedding in the lower half of the diatomaceous earth was apparent in the field (Fig. S2). Post-depositional features include the formation of channel voids as a result of plant activity, as evidenced by preserved root tissues. Bioturbation features are also present. These features, along with phytoliths become more abundant towards the top of the stratum. The uppermost 30 cm of stratum 4 is calcareous in composition with a microcrystalline calcite matrix and coarse inclusions of rounded carbonate clasts and shell, as well as fine inclusions of diatoms and phytoliths. Large channel voids and burrows in the middle portion of stratum 4 contain calcareous materials that have moved downwards.

The sedimentary characteristics of strata 3 and 4 in Locality 1 are consistent with the exposure and weathering of a surface, followed by initiation of standing water conditions, followed by development of a wetland. The changes in the sedimentary fabric and abundance of phytoliths and organic material relative to diatoms indicate that the wetland environment shifted over time, with an increase in the abundance of plants coupled with perhaps more seasonally arid conditions. Bioturbation locally moved finer material both upwards – at the contact between strata 3 and 4 – and downwards, with calcareous material from the upper 30 cm filling macrovoids in the underlying sediments. Upper stratum 4 represents a shift in the chemistry of the wetland in this area to more alkaline conditions. The resulting calcareous sediment capped the earlier siliceous wetland deposits; recrystallization and cementation of this facies likely

contributed to the preservation of the Locality 1 sequence.

In the exposures around Locality 1 and on the uplands beyond those exposures, two key strata are especially significant to the archaeological record: stratum 2 and an overlying carbonate (Figs. 2, S2, S4). In nearby exposures, upper stratum 2 is strongly modified by pedogenic weathering, characterized by a Bt-Bk soil profile (Table S2). The overlying carbonate is thickest and most continuous in proximity to Locality 1 and thins out upslope to the southeast, south, and south west. The carbonate is subdivided vertically into three zones based on physical appearance: a Lower Massive Carbonate, a Middle Platy Carbonate, and an Upper Massive Carbonate. These carbonate layers are weathered by fracturing and dissolution. The Lower Massive carbonate is the least weathered and most horizontally extensive layer. Remnants of the Middle Platy layer are common, The upper Massive Carbonate is preserved in Locality 3 where the only complete section of the carbonate sequence is preserved (Fig. S4).

Based on field observations, this carbonate sequence overlying the Big Red soil appears to be a surface accumulation of carbonate resulting from springs or seeps. This interpretation is based on several lines of evidence. The carbonate is a relatively soft, low density material, probably because it does not engulf older sediments (except at its base) as do pedogenic or groundwater carbonates. It is more likely a surface precipitate. Radiocarbon dating of succinids (see below) from the carbonate zones in Locality 3 show that the layers are time equivalents of strata 3 and 4 in Locality 1. The Lower Massive Carbonate zone yielded dates of ~16,010 and 15,060 ^{14}C years BP, and the Upper Massive layer dates ~8000 ^{14}C yrs BP, discussed below (Table S8). A likely scenario is that the seeps/springs that produced the carbonate also fed water into the strata 3/4 channel. The differences in the two sedimentary sequences are thus attributable to lateral facies changes.

Table S1: Stratigraphic Field Description, Locality 1
Profile 07-2; north side of locality at E153 line (see text Figure 3)

Stratum	**Thickness, cm**	**Soil Horizon**	**Description***
4	10-15	Lma/C	10YR 7/1 or 7/2d 6/2m; heavily weathered "lumpy" surface zone; marl-like primary carbonate mixed with diatomaceous sediment; micro-karst; very hard; abrupt boundary
	17	Bk1	10YR 7/2d 6/2m; very hard; indurated diatomaceous earth; common carbonate films on ped faces; weak prismatic & moderate subangular blocky structure; clear boundary
	18	Bk2	10YR 7/1.5d 6/2m; hard; indurated diatomaceous earth; faint, common carbonate films on ped faces; weak subangular blocky structure; clear boundary
	37	Ldi1	2.5Y 6.5/1d 5/1m (lower half is 7/1d 6/1m); soft, massive; lower half locally displays faint bedding with darker and lighter (more diatomite) horizontal lenses; scattered Succinids 10-12 cm below top of this zone throughout excavation area; abrupt, irregular lower boundary
	8	Ldi2	10YR 8/1; **diatomite**; locally laminated (1-2mm thick laminae); locally mixed with darker diatomaceous earth (visible bioturbation); upper contact is erosional; lower boundary abrupt, smooth
3B	10-15	2C1	2.5Y 7/2d 6/3m; coarse sandy clay loam with few pebbles; fine, strong

			prismatic structure due to desiccation (nonpedogenic); diatomaceous earth locally fills cracks; abrupt, wavy boundary
3A	30-50	2C2	2.5Y 7/2d 5.5/3m; massive coarse sandy clay loam with common pebbles and cobbles; discontinuous cobble lens at base; abrupt, wavy boundary
2	25	3C3	5Y 8/2d 6.5/3m; very coarse sandy clay with rare fine pebbles; fine, strong prismatic structure (non pedogenic); clear, wavy boundary
	70+	3C4	5Y 8/2d 6.5/3m; lower half mottled with 2.5YR 4/3.5d 4/4m; coarse sand; mostly massive with subangular blocky partings in upper 20 cm

*Following standardized terminology (*4*,*5*,6); Color = Munsell, d = dry; m = moist

Table S2. Stratigraphic Field Description, Locality 3
Profile 07-5; southwest corner of locality (see text Figure 1)

Stratum	**Thickness, cm**	**Soil Horizon**	**Description***
Upper massive carbonate	0-50	C1	10YR 8/2-7/2d, 5/2m; massive, hard carbonate; heavily pitted surface; clear, smooth boundary
Middle platy carbonate	50-65	C2	10YR 8/2-7/2d, 5/2m; platy carbonate with plates each 1-2cm thick; clear, smooth boundary
Lower massive carbonate	65-90	C3	10YR 8/2-7/2d, 5/2m; massive, hard carbonate; heavily pitted surface; abrupt, smooth boundary
2	90-150	Btb1	sandy clay loam, 5YR 3/4m; weak, coarse prismatic & coarse, medium subangular blocky structure; patchy, thin clay films on ped faces; clear, smooth boundary
	150-165	2Btk1b1	sandy clay loam with medium sand, 5YR 4/4m; common, fine silica pebbles; strong, coarse prismatic & strong, coarse, subangular blocky structure; continuous, thin clay films on ped faces; common carbonate films & threads on ped faces; clear, smooth boundary
	165-185+	3Btk2b1	sandy clay loam with medium sand, 5YR 4/4m; strong, coarse prismatic & strong, coarse, subangular blocky structure; continuous, thin clay films on ped faces; common carbonate films & threads on ped faces; clear, smooth boundary

* see Table S1 for notes

These hypotheses are confirmed by micromorphological analyses of samples of the Big Red soil and overlying carbonate layers in Locality 3. Here, the Big Red soil contains redoximorphic features, including gleying, which impacted the clay component. The contact between the Big Red soil and the overlying Lower Massive carbonate layer is sharp, although sand-sized materials that are similar in composition and texture to those that are present within

the Big Red soil, as well as stratum 3 in Locality 1, are present as inclusions. Microscopic redoximorphic features, such as dendritic orthic nodules of manganese oxides are present. The microstructure and morphology of the Lower Massive carbonate are inconsistent with a pedogenic origin. Pendants and calcified plant tissues are absent, although the presence of channel voids and possible infilled insect burrows indicate a degree of subaerial exposure during formation. The Middle Platy carbonate contains fewer inclusions of sand-sized materials as well as fewer secondary redoximorphic features relative to the underlying Lower Massive carbonate. Abundant, shells and intact diatoms are present within a matrix of microcrystalline calcite. Infilled chamber voids, and channels containing mineralized remnants of roots indicate subaerial exposure. The Upper Massive carbonate also contains shell fragments and diatoms, but exhibits more abundant structural features that are suggestive of bioturbation and surface weathering.

Combined, the three types of carbonate formed after the development of the Big Red soil, when a high, alkaline water table – likely associated with a seep or spring – caused the localized formation of a groundwater carbonate and alteration of the underlying sediment. Later palustrine conditions resulted in the deposition of the upper two carbonate layers, each with diatom inclusions indicative of low energy water, and post-depositional features that suggest periodic or perhaps seasonal surface exposure and occupation of the wetland by plants. The micromorphological analyses of both the siliceous and calcareous sediments of Locality 1 stratum 4, and the carbonates of Locality 3 suggest that both areas experienced an abrupt increase in surface and near-surface moisture followed by fluctuating conditions. Radiocarbon ages indicate that the resulting wetland persisted for at least six thousand ^{14}C years.

Distribution of Bones and Stones

The archaeological character of the upper bone bed in Locality 1 was essentially confirmed upon site discovery when we were able to "fit" the scraper (#45980; Fig. 9A,E) into the "mold" it left in the bone bed after the artifact had fallen out (Fig. S11). During excavation, however, the bone from the upper bone bed along with many stone artifacts were not on the same plane on or within upper stratum 3B. This was due to the gentle westward dip of the feature and the strata 3/4 contact as well as presence of some stone and bone material in upper 3B rather than at the top (Table S6; Figs. S5, S6). Examination of depth data and back plots of all material recovered (Table S6; Fig. S6) shows that the bone and stone as well as the charcoal tend to be (but are not exclusively) concentrated in a zone ~15cm thick from the top of 3B down; some is as much as 26cm deeper than the bone concentration. The deeper material likely was moved down due to cracking subsequent to formation of the main bone feature. Visible cracks within 3B were obvious and pervasive in the field (Figs. S2, S10), but were significantly less abundant in the immediately overlying sediments of stratum 4 (text Fig. 2). Similar microscopic differences between the two strata in the abundance and types of voids were observed in thin section. This distribution clearly indicates a phase of subaerial exposure of upper 3B prior to burial. Further, small fragments of bone and teeth are scattered through the upper 26cm of 3B. These data suggest that smaller items such as bone bits, charcoal fragments, and stone artifacts moved down as cracks formed whereas larger bone and bone fragments were not likewise transported.

Stone Artifacts

The artifacts found in and around the Locality 1 excavations are described and illustrated in the main text (Figs. 4, 5). Metrics on those artifacts and additional illustrations are presented here (Table S3; Figs. S7-S10).

Table S3. Artifacts from in and around the Locality 1 bone bed.

Artifact	**Raw Material with Munsell color**	**Length, mm**	**Maximum Width, mm**	**Thickness, mm**
Points, in situ				
62942, distal fragment	Light red & reddish gray chert (10R 5/2 & 6/1)	---	---	7.47
62943, complete	Brown & light brown chert (7.5YR 5/3 & 6/4)	41.2	16.52	5.99
63008, complete	Pink red & pinkish white chert (10R 6/3 & 8/2	46.1	18.4	5.99
63177, complete	Reddish brown rhyolite (2.5YR 5/3)	95.3	30.35	8.4
Points, disturbed context				
46023, complete	Light gray & gray chert (10YR 7/1 & 6/1)	88.1	29.0	7.95
58342, complete	Clear quartz	49.1	22.3	4.8
59569, complete	Brown chert (7.5YR 5/2)	52.4	18.0	6.38
Other tools, disturbed context				
45980, lateral scraper	Pale yellow chert (2.5Y 7/3)	90.5	75.2	20.7
46021, biface, distal end	Pinkish gray rhyolite (5YR 6/2)	91.2	43.4	16.4
46022, biface, midsection	Clear epidoted quartz	32.2	---	10.4
Modified bone		**Diameter, mm**		
59892, incised sphere	Bone	9.16		
59884, sphere	Bone	11.85		

Thirteen Clovis points and point fragments were collected from the surface of the upland camp area (Localities 2,5,8,9, 10, 22) (Fig. 1). Eight are basal fragments; four are complete Clovis points (two with a basal ear broken); and one middle fragment. Six points showed reuse and reworking, probably by Archaic people. Four different kinds of raw materials were employed to manufacture the points. Five were made on chert, five on the local rhyolite, two on quartzite, and one on obsidian (Table S4).

Seven projectile points and fragments were recovered from Locus 5. A complete Clovis point (#59332; Fig. S12F) was once larger, but when the tip broke, it was reworked into a new tip. This tip was used as a drill in its final incarnation. Clovis point #59083 (Fig. S12J) is complete but in halves. The two fragments were found in proximity to one another. The absence of a concave base and grinding on the base and sides, indicates that it was never used and possible never completed. Artifact #59604 (Fig. S12G) is an almost complete Clovis point

missing just one basal ear. It was heavily reworked and the tip was transformed and used as a triangular drill. Three basal fragments of Clovis points were recovered, all exhibiting distinctive fluting on both faces: artifacts #59082 (Fig. S12C), #59603 (Fig. S12A), and #59307 (Fig. S12M). Artifact #59145 (Fig. S12H) is the midsection of a Clovis point with a heavy patina. The point was reworked at least two times: darker patina covers a group of scars and a light patina covers other scars.

Table S4. Points from upland surface contexts.

Loc	Artifact	Raw Material with Munsell color	Length, mm	Maximum Width, mm	Thickness, mm
2	59287*	Rhyolite; weak red (10R 4/3)	31.25	26.35	7.23
5	59082	Chert; light reddish gray (2.5YR 7/1)	28.88	26.86	7.38
5	59603	Chert; light grey (10YR 7/2)	22.15	27.46	7.93
5	59145	Obsidian; very dark gray (7.5Y 3/1)	29.68	19.61	5.34
5	59332	Quartzite; brown (7.5YR 4/3)	44.01	27.13	7.17
5	59604	Rhyolite; dusky red (10R 3/2)	37.1	24.40	6.3
5	59083	Reddish grey (5YR 5/2)	66.33	30.66	8.56
5	59307	Chert; light brown (7.5YR 6/4)	34.86	27.22	7.49
8	59593	Chert; light grey (10yr7/2)	31.12	25.59	5.59
9	59727	Rhyolite; pale red (10R 6/3)	48.52	23.02	7.19
10	63220	Chert; gray (7.5YR 5/1)	14.75	24.81	6.28
10	63233	Rhyolite; light reddish brown (5YR 6/3)	27.03	35.30	93.41
22	63360	Rhyolite; reddish brown (2.5YR 5/3)	36.44	32.20	9.32

* Artifact recovered from a heavily eroded area north of Locality 1.

Two Clovis artifacts were found in Locus 10. Artifact #63220 (Fig. S12D) is the proximal end of a Clovis point with a concave base. Artifact # 63233 (Fig. S12L) is a Clovis basal fragment. The base is straight and does not exhibit grinding on the base or sides. The point appears unfinished and apparently broke in the final stages of the manufacture.

Localities 2, 8, 9, and 22 (Fig. 1) produced one point each. Specimen #59287 (Fig. S12E) from Loc 2 is a basal fragment of a Clovis point, fluted on both sides. The point was modified, probably with the intention of making an Archaic point. In Locality 8, point #59593 (Fig. S12B) is a basal fragment. Both sides are fluted and it has a concave base. In Locality 9, artifact #59727 (Fig. S12I) is a complete Clovis point. It is missing a basal ear and the tip was modified and used as a triangular drill. Clovis point #63360 (Fig. S12K) from Loc 22 is a basal fragment. The base is straight and does not have grinding on the base or sides. It likely broke at the final stages of the manufacture.

The upland localities and the gomphothere feature (Loc 1) appear to be related because the artifacts of both Loci have several lithic raw materials in common, and overall the Clovis points at both localities shared many technological aspects, such as same type of basal concavity and size. A Clovis point and a flake found in situ at Locus 1 were made on the local rhyolite, at the camp area five Clovis points were made of the same rhyolite. A Clovis point, a middle fragment of a biface, and three flakes were made on quartz crystal at Locus 1, and there are two dozen flakes and three biface fragments mad on quartz crystal at the camp area. At the camp area

two Clovis points were made on brown quartzite and at Locus 1 two flakes found in situ are made of brown quartzite.

A wide array of chalcedonies and cherts were used to make the end scrapers. Only one was made with local rhyolite and there is one on obsidian. The blades were made on a diverse collection of raw materials including local rhyolite, several chalcedonies and cherts. Four blades and two core tables recovered at the camp area were made on a vitrified basalt that appear to be identical to the source located at El Bajio Clovis site at about 180 kilometers to the east.

The Bone Bed

Bone concentration #1 included astragali, phalanxes, and metapodials showing fused joints. Other bones from #1 included vertebrae, long bones, a complete pelvis with both illiums present and intact ischiums and acetabellums, and foot bones. Bone concentration #2 included a mandible and a few molar fragments, pelvis, ribs, vertebra, scapula, and cranial fragments.

Strong weathering of the Gomphothere remains is illustrated by the heavily pitted, checkered, and fibrous surfaces, along with desiccation cracks and exfoliation. Some bones show carnivore tooth punctures, furrowing, and trampling marks.

Table S5. Inventory of bone from the two concentrations.

Gomphothere No 1			**Gomphothere No 2**		
Field No.	**Depth, cm**	**Description**	**Field No.**	**Depth, cm**	**Description**
58969	11.79-11.87	Radius epiphysis		11.96-11.98	group of ribs
58965	11.80-11.86	pelvis	59203	11.99-12.01	flat bone fragment
58972	11.92-11.94	Ribs	59291	11.96-12.03	Bone fragments assoc w pelvis
58988	11.96-11.98	ribs	59448	12.0	Vertebra
58989	11.88	ribs	59289	11.92-11.93	Pelvis fragments
58987	11.91-11.97	large rib (90cm)	59290	11.93-11.95	Ribs
58964	11.88-11.96	Vertebra		11.91-11.95	Vertebrae neural spine (70cm)
58986	11.85-11.89	fragment of long bone	59292	11.95	Pelvis
58983	11.83-11.86	fragment of pelvis & vertebra	59299	11.92-11.96	flat bone fragment
	11.88-11.92	Pelvis fragment	59462	11.94-11.96	long bone (30 cm)
59050	11.92	Phalange	59442	11.84-11.92	concentration of cranial fragments
46246	11.86-11.92	Phalange	58785	11.89	axis vertebra
58957	11.92-12.00	Phalange	59786	11.82-11.91	Mandible with intact premolars and M1
59049	11.94	Phalange	59787	11.91-11.93	mandible fragments with teeth frags
58984	11.81	Phalange	59415	11.91-11.95	Ribs
59110	11.91-11.97	Phalange	59419	11.91-11.95	Ribs
58965	11.87-11.91	Long bone		11.97-98	vertebra

58964	11.88-11.97	Vertebrae		11.88-11.92	long bone (40cm)
59132	10.84	Vertebrae		11.93	Rib
	59780	11.88-12.02		11.92-11.96	Rib
			59780	11.88-12.02	Scapula

Table S6. Depths* of stone artifacts, bones, and charcoal from the Upper Bone bed at Locality 1 relative to the strata 3/4 contact[1]

Units 148-150E											
543N			**544N**			**545N**			**546N**		
Item	Depth, mbd	3/4	item	Depth, mbd	3/4	item	Depth, mbd	3/4	item	Depth, mbd	3/4, mbd
					11.82	flake	12.06	11.82			11.82
Units 150-152E											
G 1			***G 1***								
B Frag	11.81.11.91	11.82	B Frag	11.96-11.98	11.82-11.88	flake	11.88	11.82	flake	11.86-11.96	11.82
Pelvis	11.80-11.86		B Frag	11.81-12.01	11.82-11.88				**CHARC**	12.06	11.82
Ribs	11.92-11.94	11.82	B Frag	11.88-11.92					flake	11.86-11.96	11.82
	11.96-11.98	11.82-11.88									
	11.88	11.82-11.88									
Flake	11.90	11.82									
CHARC	12.10	11.82									
Units 152-153E											
G 1			***G 1***			***G 2***			***G 2***		
rib	11.91-11.97	11.91-11.92	point	11.96-11.97	11.91-11.93	clavicle	11.83-11.92	11.91			
Vert	11.88-11.96	11.91-11.92	Rounded bone	11.96-12.04	11.91-11.93						
phalange	11.94										
Phalange	11.98-12.02										
phalange	11.86-11.98		phalange	11.86-11.98							
Flake	11.91	11.91-11.92									
Units 154-155E											
			G 2			***G 2***			***G 2***		
flake	12.05-12.10	11.93-11.99	Burned bone	11.99-12.07	11.94-12.09	B frag	11.99-12.01	11.91-11.93	ribs	11.93-11.95	11.91-11.93
flake	12.05-12.10	11.94	Xtal flake	12.09	11.95	pelvis	11.96-12.03	11.91-11.93	bone frag	11.91-11.95	11.91-11.93
						vert	11.99-12.02	11.91-11.93	pelvis	11.95	11.91-11.93

									Bone frag	11.92-11.96	11.91-11.93
									flake	12.02-12.07	11.91-11.93
									flake	11.89-11.99	11.91-11.93
									flake	11.89-11.962	11.89
Units 156-157E											
			G 2			***G 2***			***G 2***		
flake	12.56-12.75	12.0-12.02	bone frag	11.91-12.04	11.88-11.93	vert	11.97-11.98	11.88-11.93	flake	12.02	11.99
			skull bits	11.84-11.92	11.88-11.93	B frag	11.88-11.92	11.88-11.93	flake	12.02-12.07	11.89
			vert	11.89	11.88-11.93	rib	11.93	11.88-11.93			
			mandible	11.82-11.97	11.88-11.93	mandible	11.86-11.95	11.88-11.93			
			Mandible frags & teeth frags	11.90-11.96	11.88-11.93	ribs	11.92-11.96	11.88-11.93			
			point	12.14	11.88-11.93	Scapula	11.88-11.98				
			Xtal Flake	11.95	11.88-11.93						
Units 158-160E											
			point	12.06	11.97-12.04	point	12.06	11.07			
			flake	11.96		2 flakes	12.15				
						2 flakes	11.90				

*mdb = depth in meters below datum.
Table is organized following the grid system used in the Locality 1 excavation area (see text Fig. 3): south to north across the top (543N to 546N) and west to east from top to bottom (148E to 160E); G1, G2 indicates the excavation units with Gomphothere 1 and Gomphothere 2, respectively.
CHARC = radiocarbon dated charcoal.

Radiocarbon dating

Radiocarbon ages from El Fin del Mundo were determined on charcoal, shell, and organic matter in sediment. Charcoal was found in the upper part of Stratum 3B, and at the base of the Diatomaceous Earth, along its contact with the Diatomite in Stratum 4. Fossil Succineidae (pulmonate semi-aquatic gastropods with shells reliable for radiocarbon dating, *7,8*) and Gyraulus (pulmonate aquatic gastropods) were recovered from upper Stratum 4, and from the carbonate overlying Stratum 2 on the surrounding uplands. Throughout the Diatomaceous Earth are high levels of organic matter. Observations of thin sections (by SMM) indicate that the majority of the organic matter is present in primary depositional lenses containing clay, phytoliths and diatoms, in addition to humified plant tissues (see Fig. S3c). Younger and some modern organic material is present in channel voids and sources from degraded plant roots. Calibrated radiocarbon ages (Cal BP) are given as the 2σ range and median probability of possible calendar year ages, following
Calib 7.0: http://calib.qub.ac.uk/calib/ and IntCal13 (*9*).

Charcoal: Stratum 3B

Five specimens of fragmented carbonaceous material were gathered from the upper 15cm of Stratum 3B in the same area as the Gomphothere bone bed/Clovis level (Figs. S14, S15). Examination by AK under binocular microscope revealed preservation of woody tissue structure in only two of these specimens, but their high degree of fragmentation precluded taxonomic identification upon further examination by paleoecologist Owen Davis (U. of Arizona). Dating efforts were focused on the only confirmed charcoal specimens, FdM#63447 (AA-100181) and FdM#63176 (AA-100182), which were also the only two specimens large enough to produce reliable ^{14}C dates. Using a stainless steel probe and binocular microscope, AK separated sub-millimeter size charcoal splinters from the enclosing sediments until just above 1.2 mg was obtained from each specimen. Samples were subsequently handled by senior staff scientist TL in the Arizona AMS facility per small sample protocol provided by AK, described in the following section.

Pretreatment

Charcoal samples were pretreated in combustion tubes, and subsequent weighing was avoided, so as to minimize sample loss or introduction of particulate contaminants prior to the combustion step. Samples were pretreated in accordance with a standard acid–base–acid protocol. The first acid (10% HCl) step removes inorganic carbon (bound in carbonate salts) and acid-soluble organic molecules. The base (2% NaOH) step produces a suspension of humic acid (B-fraction) that is subsequently decanted from the treated charcoal (A-fraction), and recovered by flocculation upon final acidification with HCl. For A-fraction, a final acid wash ensures removal of modern C, introduced during the base step. Following the final acid step, A-fractions are rinsed in deionized water and both fractions dried *in vacuo* in preparation for combustion. Of the two pretreated specimens, only FdM#63447 (AA-100181) yielded both A- and B-fraction, while FdM#63176 (AA-100182) yielded only B-fraction (Table S7). Several "radiocarbon-dead" charcoal standards (Rio Frio Ash), henceforth referred to as "blanks", were simultaneously processed.

Background Levels and Process Blanks

Laboratory contamination can occur during wet chemical pretreatment via introduction of solid phase contaminants of sufficient mass and age relative to the sample, although strict measures are taken to minimize this. On the other hand, contamination consistently occurs during cryogenic purification (or "extraction") of CO_2 following sample combustion, when the sample comes into contact with extraneous C in the form of CO_2 and other, less abundant organic compounds—significantly impacting the measured ^{14}C activity of a given sample. The background level acquired during extraction depends on the quantity and ^{14}C activity of contaminant C relative to the size and age of the sample. Contamination is introduced primarily through admixture with modern CO_2 entering the vacuum line through leakage, and exchange with CO_2 of unknown age, adsorbed onto O-rings and other parts of the line. At the Arizona AMS facility, background levels are quantified and expressed as the fraction of modern carbon, based on the long-term average measured from process blanks (*9,10*). Background levels within the accelerator, comparatively negligible under normal circumstances, are measured independently with unprocessed "machine" blanks.

Small Sample Effect

The above considerations suffice for assessing background levels in samples larger than ~0.5 mgC, while additional uncertainties impact smaller samples—collectively referred to as the "small sample effect." First, the influence of background levels on sample ^{14}C activity is inversely proportional to sample size, causing disproportionate underestimation of age and increased scatter in samples <0.5 mgC. Each laboratory must calibrate this effect with a set of analyses on blanks of different sizes, as described for the Arizona AMS facility (10) and elsewhere (e.g., *11,12*). Additional issues arise in samples <0.2 mgC, for which various laboratories have reported fractionation resulting in lower apparent ^{14}C activity. This fractionation stems from reduced and variable ion source efficiency as it affects the influence of beam current intensity on the iron catalyst (e.g., *13,14*) bound with sample C in its reduced form as iron carbide, or "graphite". This can result in age overestimation and increased scatter, and is inversely proportional to sample size. Because fractionation cannot be detected with blanks, each laboratory must calibrate this effect with a series of analyses on standards of different masses. All dates for samples <0.5mgC reported by the Arizona AMS Radiocarbon facility were corrected for the small sample effect which, when coupled with conservative error propagation, ensure the accuracy of resultant ^{14}C dates within 1σ. This leaves room only for improvement in precision, which can be accomplished by simultaneously processing and analyzing blanks and standards that match in size with the sample.

Results and Technical Considerations

To optimize precision, we performed extractions on the "cleanest" vacuum line (i.e., exhibiting the lowest background levels) following at least a 24-hour pump-down period and attempted to process unknowns and matching-size blanks simultaneously. To avoid unnecessary reduction in sample size and additional related uncertainties, we measured $\delta^{13}C$ on the same CO_2 aliquots used for radiocarbon analysis. C yields and measured fMC values for samples and blanks are reported in Table S7, and the dates we calculate using background levels measured from these blanks, in addition to dates reported by the Arizona AMS facility using the standard procedures described by Donahue et al. (*10*), are listed in Table S7. For the A-fraction of

charcoal sample FdM#63447 (AA-100181A), we calculate an age of 11,550±60 ^{14}C BP, preferable to the reported age of 11,560±140. Because the corresponding B-fraction (AA-100181B) was smaller than any of the blanks, we are restricted to calculating a minimum limiting age and error term (10,790±60 ^{14}C BP) and therefore defer to the reported date of 10,650±250 ^{14}C BP. Using the same approach to calculate an age for the base-soluble charcoal sample FdM#63176 (AA-100182B) yields a date of 11,940±360 ^{14}C BP, as compared with the reported date of 11,880±200 ^{14}C BP. At 1σ, all of our calculations produce non-overlapping ^{14}C BP ages that are statistically indistinguishable from those reported.

A few observations are noteworthy in light of the technical considerations outlined previously. First, we did not process any (modern) standards and therefore cannot assess the effect of machine-induced fractionation on measured fMC values. Next, since it is difficult and/or labor intensive to produce matching-size blanks, we attempted to weigh out blanks sized to bracket the mass of each sample. In the case of AA-100181A, blank V21567 was identical in size to the sample; because its measured ^{14}C activity is higher than that of another, smaller blank processed on the same day (V21568), we employ both to constrain background level variability, although the exclusive use of either blank to calculate sample age results in a discrepancy of only 40 ^{14}C yr. For both B-fractions, our method yields ages older than those reported—by 60 and >140 ^{14}C yr for AA-100182B and AA-100181B, respectively. In the case of AA-100182B, this might be explained by our use of a blank processed in a different batch, possibly experiencing slightly higher background levels. Alternatively, or additionally, these samples might have been subject to fractionation given their small sizes. Since the Arizona AMS facility accounts for these effects with size-specific corrections and error propagation based on their own calibration data set, we defer to the reported ages for these samples. On the other hand, with respect to AA-100181A we suggest that the remarkable agreement between our calculation and the reported age can be explained on the basis of sample size (0.23 mgC), which is safely above the threshold for machine-induced fractionation reported in several studies (0.15 mgC) (*12-15*).

Table S7. Sample information and uncorrected ^{14}C measurements for small charcoal and blanks.

Field#	Lab#	Chem#	Extraction	Type	Fraction	mgC	δ^{13}C	F	± (scat)	± (stat)
	-	V21567	19-Nov-12	blank	-	0.23	-22.8	0.0096	0.0008	0.0004
	-	V21568	20-Nov-12	blank	-	0.16	-22.8	0.0082	0.0004	0.0003
	-	V21841	8-Aug-13	blank	-	0.10	-22.8	0.0351	0.0015	0.0015
63447	AA-100181A	V21564	19-Nov-12	sample	A	0.23	-24.2	0.2443	0.0024	0.0016
63447	AA-100181B	V21564H	8-Aug-13	sample	B	0.08	-24.3	0.2682	0.0023	0.0018
63176	AA-100182B	V21565	19-Nov-12	sample	B	0.13	-21.8	0.2417	0.0023	0.0016

Geochronologic Interpretations

Following our evaluation of the AMS ^{14}C measurements, we are left to interpret the vetted dates with respect to the age of the upper bone bed and artifacts in upper 3B. The B-fraction extracted from charcoal is comprised of an unknown proportion of indigenous to extraneous humic acids, the latter potentially affecting apparent age of the A-fraction. Under ideal circumstances, dating of both fractions allows one to qualitatively assess the relative age of natural contamination. If both fractions have equivalent ^{14}C activities, then trace quantities of

humic acid remaining in the charcoal following pretreatment would have no influence on the apparent age of the A-fraction. On the other hand, if both fractions produce discrepant ^{14}C activities, concern over contamination is warranted.

As documented previously, only two out of five carbonaceous samples were of certain charcoal origin; both were therefore pretreated, one (FdM#63447/AA-100181) yielding both A- and B-fraction, and the other (FdM#63176/AA-100182) yielding only a B-fraction. For FdM#63447, the A-fraction (AA-100181A: 11,550±60 ^{14}C BP) was older than the B-fraction (AA-100181B: 10,650±250 ^{14}C BP)—both fractions younger than the B-fraction of FdM#63176 (AA-100182B: 11,880±200 ^{14}C BP). Considering that none of the uncalibrated ^{14}C dates overlap at 1σ, the results of paired-fraction dating for FdM#63447 render the A-fraction date of 11,550±60 ^{14}C BP (13,384 +105/-119 Cal BP) a minimum age under the unlikely circumstances that the pretreatment was not fully effective. In contrast, it is impossible to evaluate the reliability of data from the other charcoal sample (FdM#63176/AA-100182), since it was 100% base-soluble—and was therefore incorporated into the B-fraction during pretreatment. However, we note that its 2σ calibrated age range (13,733 +496/-454 Cal BP) overlaps with that of FdM#63447, stimulating speculation about an earlier occupation. Likewise, a date of 11,040±580 ^{14}C BP (12,854 +1,411/-1,666 Cal BP) on an isolated lump of organic matter from mid-to-upper 3B (FdM#59354/AA-83272B), processed by GH before the charcoal samples were unearthed, may reflect a much younger Clovis component. Unfortunately, the large error and other uncertainties surrounding these dates render them intriguing at best. As is, AA-100181A the only reliable date from the Clovis level.

Use of matching-size blanks has allowed us to confirm the accuracy of the A-fraction age reported for charcoal sample FdM#63447 (AA-100181A), and to improve its precision by a factor of >2, while paired-fraction dating has enabled us to confirm the antiquity of the charcoal. The importance of improved precision becomes clear once its impact on the 2σ calibrated age range is considered, causing a ~150 Cal yr raise in the lower limit—from 13,112 to 13,265 Cal BP—using Calib 7.0. Lastly, a substantial reduction in the standard deviation of this and other dates could significantly affect the summed probability distribution of Clovis dates throughout North America, particularly with respect to smaller geographic subsets.

Shell Dating

Shells for dating were collected from the Lower Massive Carbonate in winter/spring 2008, and those from Strata 3 and 4 were collected between December 2008 and January 2011. Upon collection, shells were moderately encrusted and infilled with carbonate-rich sediment. Depending on their resilience, specimens were briefly sonicated (2-5 seconds) up to 3 times prior to a final rinse with distilled water. Next, they were crushed, and both interior and exterior surfaces inspected for adhering detritus under binocular microscope. Finally, clean fragments were selected and, if more sample was required for dating, some of the remaining fragments were etched in a dilute acid solution (0.01% HCl). All shells were processed by AK at the Arizona AMS Radiocarbon facility, on the extraction line of Jay Quade.

Table S8: Radiocarbon dates from Localities 1 and 3, El Fin del Mundo.

Unit	Member+	Zone	Lab #	Sample Type	Fraction ++	^{14}C yr BP#	±	Cal yr BP range (2σ)#			δ^{13}C (‰ VPDB)
								median	+	-	
Locality 1											
Stratum 4	D.E.	upper	†AA-88885	shell (Succinid)	NA	**8,870**	60	**9,993**	191	255	-6.2
Stratum 4	D.E.	mid-to-upper	†AA-81350	shell (Succinid)	NA	8,030	50	8,892	138	233	□□□
Stratum 4	D.E.	mid-to-upper	†AA-88886	shell (Succinid)	NA	8,470	50	9,490	51	71	-6.3
Stratum 4	D.E.	lower	A-14837	O.M.	A	8,375	110	9,357	183	318	-21.8
Stratum 4	D.E.	basal contact	A-14850	O.M.	A	9,030	75	10,193	187	281	-24.3
Stratum 4	D.E.	lower	A-14836	O.M.	A	9,465	100	10,752	384	312	-17.1
Stratum 4	D.E.	basal contact	‡AA-80085B	charcoal	B	9,290	290	10,529	718	856	-13.2
Stratum 4	D.E.	basal contact	‡AA-80671B	charcoal	B	9,560	120	10,901	301	326	-22.9
Stratum 4	D.E.	basal contact	AA-80084A	charcoal	A	**9,715**	64	**11,136**	109	344	-13.2
Stratum 4	D.	base	A-14896A	O.M.	A	6,185	115	7,076	332	318	-17.9
Stratum 4	D.	top	AA-80078A	O.M.	A	6,921	58	7,756	170	100	-24.6
Stratum 4	D.	upper	AA-80076A	O.M.	A	7,570	93	8,376	168	189	-25.1
Stratum 3	3B	upper	AA-100181A	charcoal	A	11,560	140	13,384	320	272	-24.2
"	"	"	†AA-100181A	"	"	**11,550**	**60**	**13,384**	**105**	**119**	"
Stratum 3	3B	upper	AA-100181B	charcoal	B	**10,650**	**250**	**12,486**	**584**	**729**	-24.3
"	"	"	†AA-100181B	"	"	>10,790	>60	>12,706	>83	>83	"
Stratum 3	3B	upper	‡AA-100182B	charcoal	B	**11,880**	**200**	**13,733**	**496**	**454**	-21.8
"	"	"	†‡ AA-100182B	"	"	11,940	360	13,909	1152	807	"
Stratum 3	3B	mid-to-upper	‡AA-83272B	O.M.	B	11,040	580	12,854	1,411	1,666	-17.8
Stratum 3	3B	Upper	□□AA-95550	tooth enamel	NA	9,804	93	-	-	-	-5.6
Stratum 3	3B	Lower	□□AA-95550	tooth enamel	NA	9,755	92	-	-	-	-5.3
Stratum 3	3A	Middle	†AA-90707	shell (Planorbid)	NA	≤12,180	40	≤14,071	130	131	□□□
-	-	disturbed portion	†AA-94054	shell (Succinid)	NA	8,850	40	9,969	189	224	□□□
-	-	nearby well	AA-92972	groundwater	DIC	1,180	30	-	-	-	NA
Locality 3											
Carbonate	Upper	Top	†AA-94057	shell (Succinid)	NA	**8,000**	40	**8,875**	134	158	□□□
Carbonate	Lower	Upper	†AA-81042	shell (Succinid)	NA	**15,060**	50	**18,303**	167	205	□□□
Carbonate	Lower	Middle	†AA-81043	shell (Succinid)	NA	**16,010**	80	**19,323**	232	256	□□□

* Suffix indicates A or B fraction of organic carbon;

** dates reflect diagenesis and were thus left uncalibrated; see text

*** An estimated δ^{13}C value (-5‰) was used to adjust measured ^{14}C activity for biologic fractionation

† Age calculated on the basis of sample-specific extraction blanks, as explained in text; all other dates reflect the long-term (~1 yr) average

‡ Dates of B-fraction from 100% base-soluble samples; # Bold = preferred age estimate;

+ D. = Diatomite; D.E. = Diatomaceous Earth; ++ DIC = dissolved inorganic carbon.

Key assumptions in the radiocarbon dating of shell are that the initial ^{14}C content of the shell aragonite was equivalent to that of atmospheric CO_2 at the time of shell growth, and that open-system behavior has not occurred since that time. The first warrants additional consideration with respect to potential sources of ^{14}C-depleted carbon, which may have initially been incorporated into the shell to cause a ^{14}C reservoir effect. Specific concern over this issue arises if age data are acquired from terrestrial and semi-aquatic gastropods, since certain taxa are known to incorporate significant amounts of inorganic carbon into their shells (the "limestone problem" after Goodfriend and Stipp, *16*). Most Succineidae spp. grow shells equivalent in ^{14}C activity to the atmosphere, thus providing reliable ^{14}C age data. However, because malacologists cannot distinguish among genera on the basis of shell morphology alone, some concern over the limestone problem is warranted in the event that carbonate-bearing substrate is locally present. In this case, the apparent absence of carbonate substrate in the immediate uphill-adjacent vicinity of Stratum 3A significantly reduces the potential for this problem. Analogous to the limestone problem are the "hard-" and "old-" water effects (indistinguishable from one another), resulting from the fact that aquatic organisms incorporate dissolved inorganic carbon into their shells—causing a fossil snail's apparent age to exceed its true age if formed in the presence of ^{14}C-depleted water. Finally, with respect to possible open-system behavior, the results of several studies indicate that post-depositional exchange has not been observed in gastropod shells <25 ka (*8,17,18*), whereas small amounts of contamination in older samples can substantially influence measured ^{14}C activity.

Shells: Lower Massive Carbonate and Stratum 3A

Shell dates reported include three from Locality 3 (two of which are discussed in the stratigraphy section and depicted in text Figure 2) and four from Locality 1 (one of which is depicted in both Figures 2 and S2). Dates on shells from Stratum 4 and the Upper Massive Carbonate are explained in the paragraph below. Only one of the two shell dates reported from Stratum 3A dates to the Pleistocene, although it is necessary to consider a possible reservoir effect when considering the true age of the shell. To constrain this for ancient springs in southern Nevada, Brennan and Quade (*17*) used the offset in age between aquatic snails and co-occurring charcoal in channel fill, determining a larger offset for Holocene age shells in relation to their Pleistocene counterparts and suggesting shorter groundwater travel times during the Pleistocene due to increased aquifer storage. Accordingly, we regard a single date of 1,180±30 ^{14}C BP (AA-92972) on groundwater collected from a nearby well as a minimum constraint on the combined hard- and old-water effect influencing the ^{14}C activity of modern groundwater—minimum, given that we do not know the extent of exchange between dissolved inorganic carbon and atmospheric C prior to sampling.

Presuming minimal exchange, we regard the apparent age of modern groundwater as a maximum constraint on a possible reservoir effect influencing the initial ^{14}C activity of late Pleistocene age aquatic shells in Stratum 3A. Following this, a date of 12,190±40 ^{14}C BP (AA-90707), or 14,080 +130/-127 Cal BP, from an aquatic snail (Gyraulus sp.) represents the maximum age of the shell, whereas a correction using the modern groundwater date results in a date of 11,010±50, or 12,874±138 Cal BP. However, regarding the oldest date from Stratum 3B of 11,880±200 ^{14}C BP (AA-100182B), or 13,733 +496/-454 Cal BP, as a minimum date for termination of 3A deposition limits potential age bias in the Gyraulus shell to ~300±200 ^{14}C yr,

or ~350±500 Cal yr. Alternatively, using the trusted date of 11,550±60 ^{14}C BP (AA-100181A), or 13,384 +105/-119 Cal BP, from upper 3B, results in a potential age bias of ~650±70 ^{14}C yr, or ~700±170 Cal yr. In both cases, the bias is similar when translated into calendar years, roughly half that resulting from use of the observed modern reservoir effect, ~1,200±190 Cal yr. In conclusion, deposition of Stratum 3A terminated no more than ~700±170 Cal yr prior to emplacement of the bone bed, and quite possibly less given the significant possibility that Stratum 3A contains shells younger than AA-90707.

Shells, Organic Matter, and Charcoal: Stratum 4 and Upper Massive Carbonate

Dating snails, organic matter, and charcoal from the same unit enables one to assess the stratigraphic integrity of a deposit, ultimately revealing the history of its deposition and post-depositional modification, and its paleoenvironmental significance. Sedimentary organic matter is comprised of materials deposited over the course of an unknown time interval and contains fractions which decompose at varying rates; its ^{14}C age represents the "mean residence time", and is generally regarded as a minimum—excepting contexts in which older material might have been introduced into the deposit. Further, post-depositional additions of organic matter can cause heterogeneity in the apparent mean residence time. Organic matter samples were submitted for conventional or AMS radiocarbon dating at the U of Arizona's Environmental Isotope Laboratory and AMS Radiocarbon facility, respectively; all charcoal samples were processed in the Arizona AMS Radiocarbon facility.

Poor chronostratigraphic integrity best characterizes the sequence exposed at Locality 1. However, dates from reliable materials such as charcoal and shells provide a geochronologic framework within which paleohydrologic conditions can then be reconstructed, complementing information from other paleoenvironmental data sets. A date of ~9,700 ^{14}C BP (AA-80084A) on charcoal from the base of the Diatomaceous Earth, and a snail date of ~8,000 ^{14}C BP (AA-94057) from the top of the Upper Massive Carbonate bracket an interval during which phreatic discharge led to formation of these deposits. Despite a general tendency among geologists to view stratigraphic anomalies as problematic, and to selectively disregard "age outliers", we exploit both toward developing a more refined chronology of early Holocene paleohydrology and deposit formation at El Fin del Mundo. A date of ~8,900 ^{14}C BP (AA-88885) on a shell from the top of Stratum 4 likely indicates that the Diatomaceous Earth was deposited primarily during a relatively wet period between ~9,700 and ~8,900 ^{14}C BP, whereupon marsh-like conditions yielded to wet meadow conditions. At that time, organisms and vegetal matter in stratum 4 were locally bioturbated, explaining the presence of a ~8,900 ^{14}C BP snail (AA-94054) at the base of disturbed sediments at the far eastern tip of the Locality 1 island, and similar age organic matter at the base of the Diatomaceous Earth. Subsequent humid intervals interrupted an otherwise dry period, causing recurrent discharge through ~8,000 14C BP. At these times, fresh biogenic materials were introduced into the Diatomaceous Earth, as reflected by dates on snails and organic matter throughout. Concurrent discharge at Locality 3 led to incremental aggradation of carbonate until final desiccation at ~8,000 14C BP, after which Holocene aridity prevailed.

Bone and Teeth from the Upper Bone Bed

Gomphothere bone was poorly preserved. Samples obtained from the upper bone bed in Locality 1 did not yield collagen so attempts at direct radiocarbon dating of bone were abandoned. Further efforts focused on Gomphothere teeth as they appeared to be better preserved. A 3-cm long fragment of M1-Rright from the Gomphothere mandible was split open along existing fracture lines that ran from a cusp in the molar crown down to the enamel-root margin. The fragment included adhering dentin. An attempt was made to extract collagen from the exposed tooth dentin, but this also failed to yield any protein.

A strategy was adopted to try to date the Gomphothere using the enamel radiocarbon content, despite the caution expressed by others (*19*). Dentin removal exposed the inner enamel surface of the tooth (Fig. S16). Metcalfe (*20*) indicates that the inner enamel surface can provide higher resolution time-series stable-isotope data, suggesting better enamel preservation there. The inner enamel surface became the target for enamel radiocarbon dating.

Enamel was drilled from the inner surface down to a depth of approximately 0.5 mm. The drillings were divided into two portions, one from the cusp end of the fragment (distal) and the other from the enamel-root margin end of the fragment (proximal). Both samples were soaked in 2.5% NaOCl for 24 hours, followed by 0.1M acetic acid for 4 hours, to remove exogenous carbonates. The resulting powder was rinsed extensively with DI water and dried. Hydrolysis was carried out using anhydrous phosphoric acid at 70 C overnight. This protocol was developed for the treatment of tooth enamel prior to stable isotope measurement (*21*). Graphitization, measurement, and calibrations were carried out by the AMS laboratory using established protocols.

The distal inner enamel surface generated 194.8 mgs of powdered enamel and 0.95 mg of carbon for dating (0.8%C). The proximal enamel surface yielded 223.1 mg of powdered enamel and 1.28 mg of carbon (0.87%C), of which 0.74 mgs was used for dating (Table S9).

Table S9. Radiocarbon measurements from Gomphothere M1 Right enamel.

Lab No.	Sample ID	C (mg)	δ13C (‰)	^{14}C age BP	+-
AA95550	M1 right Proximal	0.74	-5.6	9,804	93
AA95550	M1 right Distal	0.95	-5.3	9,755	92

Both of the resulting dates are similar, suggesting that the enamel radiocarbon content was homogeneous throughout the tooth enamel at this crude spatial resolution. Both dates appear to be younger than expected based upon the association of the bone and teeth with Clovis points and the charcoal dates discussed above. The results suggest that the inner enamel surface is not exempt from diagenetic uptake of younger carbon. A systematic pattern of younger enamel radiocarbon dates versus collagen radiocarbon dates from the same tooth has been documented by others (*19,22*).

References Cited

1. Stoops, G., 2003. *Guidelines for Analysis and Description of Soil and Regolith Thin Sections*. Soil Science Society of America Inc..
2. Alonso-Zarza, A. M., & Wright, V. P., 2010. Palustrine carbonates. *Developments in Sedimentology* 61, 103-131.
3. Pimentel, N. L., Wright, V. P., & Azevedo, T. M., 1996. Distinguishing early groundwater alteration effects from pedogenesis in ancient alluvial basins: examples from the Palaeogene of southern Portugal. *Sedimentary Geology* 105(1), 1-10.
4. Birkeland, Peter W., 1999. *Soils and Geomorphology, 2nd Ed.* Oxford University Press.
5. Holliday, Vance T., 2004. *Soils and Archaeological Research*. Oxford University Press.
6. Schoeneberger, P. J., D. A. Wysocki, E. C. Benham, and Soil Survey Staff, 2012. *Field Book for Describing and Sampling Soils, Version 3.0.* Natural Resources Conservation Service, National Soil Survey Center, U.S. Department of Agriculture, Lincoln, NE.
7. Pigati, J.S., Quade, J., Shahanan, T.M., Haynes Jr., C.V., 2004. Radiocarbon Dating of Minute Gastropods and New Constraints on the Timing of Late Quaternary Spring-Discharge Deposits in Southern Arizona, USA. Palaeogeography, Palaeoclimatology, Palaeoecology 204(1):33-45.
8. Pigati, J.S., Rech, J.A., Nekola, J.C., 2010. Radiocarbon Dating of Small Terrestrial Gastropod Shells in North America. *Quaternary Geochronology* 5:519-532.
9. Reimer, P.J., Bard, E., Bayliss, A., Beck, J.W., Blackwell, P.G., Bronk Ramsey, C., Buck, C.E., Cheng H., Edwards, R.L., Friedrich, M., Grootes, P.M., Guilderson, T.P., Haflidason, H., Hajdas, I., Hatté, C., Heaton, T.J., Hoffmann, D.L., Hogg, A.G., Hughen, K.A., Kaiser, K.F., Kromer, B., Manning, S.W., Niu, M., Reimer, R.W., Richards, D.A., Scott, E.M., Southon, J.R., Staff, R.A., Turney, C.S.M., van der Plicht J., 2013. IntCal13 and Marine13 Radiocarbon Age Calibration Curves 0–50,000 Years Cal BP. Radiocarbon 55(4):1869-1887.
10. Donahue, D.J., Linick, T.W., Jull, A.J.T., 1990. Isotope-Ratio and Background Corrections for Accelerator Mass Spectrometry Radiocarbon Measurements. Radiocarbon 32(2):135-142.
11. McNichol, A.P., Jull, A.J.T., Burr, G.S., 2001. Converting AMS Data to Radiocarbon Values: Considerations and Conventions. Radiocarbon 43(2A):313-320.
12. Brown T.A. and Southon J.R., 1997. Corrections for Contamination Backgrounds in AMS 14C Measurements. Nuclear Instuments and Methods in Physics Research B:123-208.
13. Pearson, A., McNichol, A.P., Schneider, R.J., von Reden, K.F., Zheng, Y., 1998. Microscale AMS 14C Measurements at NOSAMS. Radiocarbon 40(1):61-75.

14. Santos, G.M., Southon, J.R., Griffin, S., Beaupre, S.R., Druffel, E.R.M., 2007. Ultra Small-Mass AMS 14C Preparation and Analyses at KCCAMS/UCI Facility. Nuclear Instruments and Methods in Physics Research B 259:293-302.
15. Klinedinst, D.B., McNichol, A.P., Currie, L.A., Schneider, R.J., Klouda, G.A., von Reden, K.F, Verkouteren, R.M., Jones, G.A., 1994. Comparative Study of Fe-C Bead and Graphite Target Performance with the National Ocean Science AMS (NOSAMS) Facility Recombinator Ion Source. Nuclear Instruments and Methods in Physics Research B 92:166-171.
16. Goodfriend, G.A. and Stipp, J.J., 1983. Limestone and the Problem of Radiocarbon Dating of Land-Snail Shell Carbonate. Geology 11:575-577.
17. Brennan, R. and Quade, J., 1997. Reliable Late-Pleistocene Stratigraphic Ages and Shorter Ground-water Travel Times from14C in Fossil Snails from the Southern Great Basin. Quaternary Research 47:329–336.
18. Rech, J.A., Pigati, J.S., Lehmann, S.B., McGimpsey, C.N., Grimley, D.A., Nekola, J.C., 2011. Assessing Open-System Behavior of 14C in Terrestrial Gastropod Shells. Radiocarbon 53(2):325-335.
19. Hedges REM, Lee-Thorp JA, and Tuross NC (1995) Is tooth enamel carbonate a suitable material for radiocarbon dating? *Radiocarbon* 37(2): 285-290.
20. Metcalfe JZ (2011) Late Pleistocene climate and proboscidean paleoecology in North America: Insights from stable isotope compositions of skeletal remains. PhD dissertation. (Univ of Western Ontario, London, ON, Canada).
21. Koch PL, Tuross N, and Fogel ML (1997) The Effects of Sample Treatment and Diagenesis on the Isotopic Intregrity of Carbonate in Biogenic Hydroxylapatite. *Journal of Archaeological Science* 24(5):417-426.
22. Surovell TA. (2000) Radiocarbon Dating of Bone Apatite by Step Heating. *Geoarchaeology: An International Journal*, 15(6):591-6

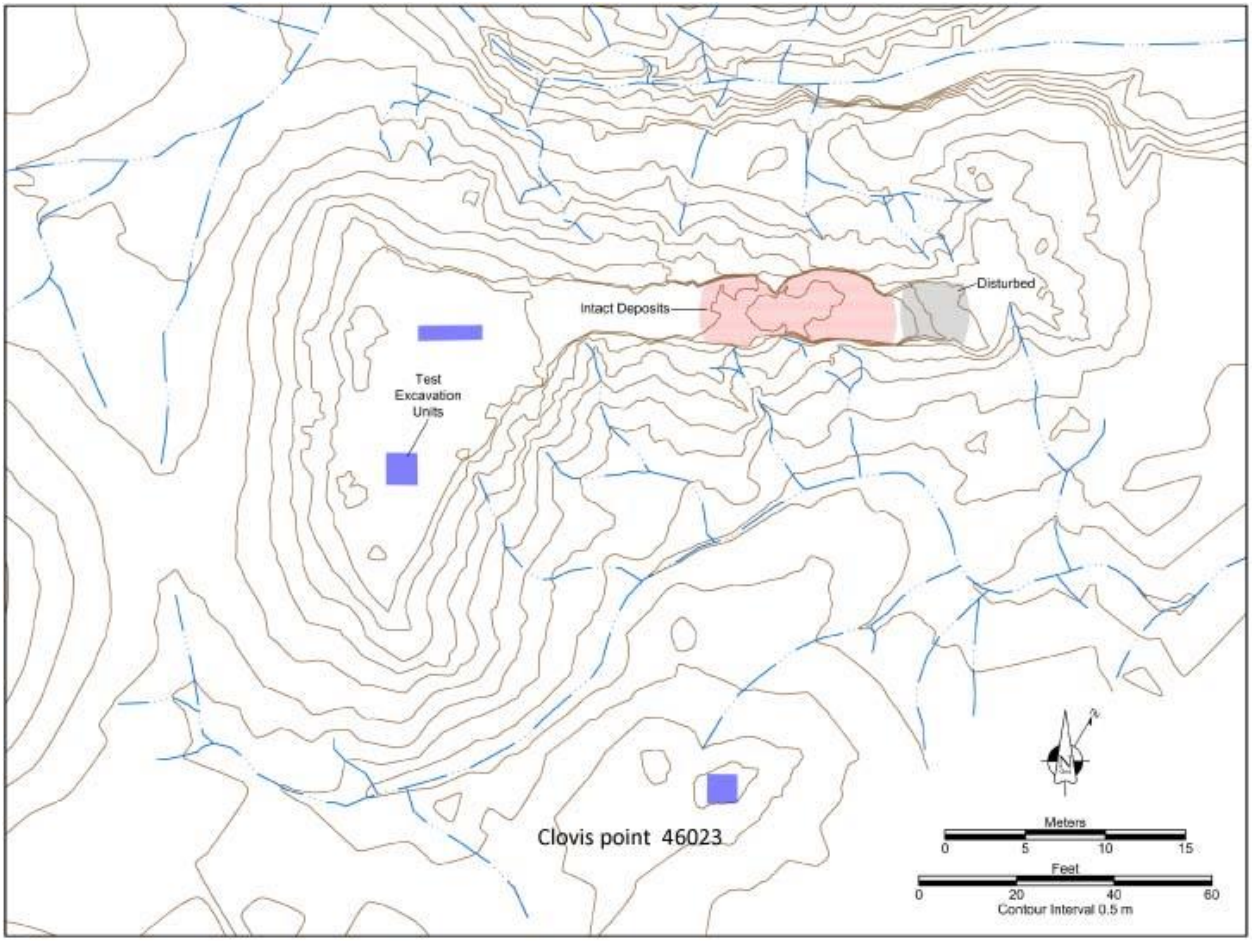

Figure S1. Topographic map of the Locality 1 "island" and surrounding area showing the main excavation area (pink), disturbed area (gray), and three test units (blue) located on the west end of the island and in the area where point 46023 (Figs. 4A, S8C) was found.

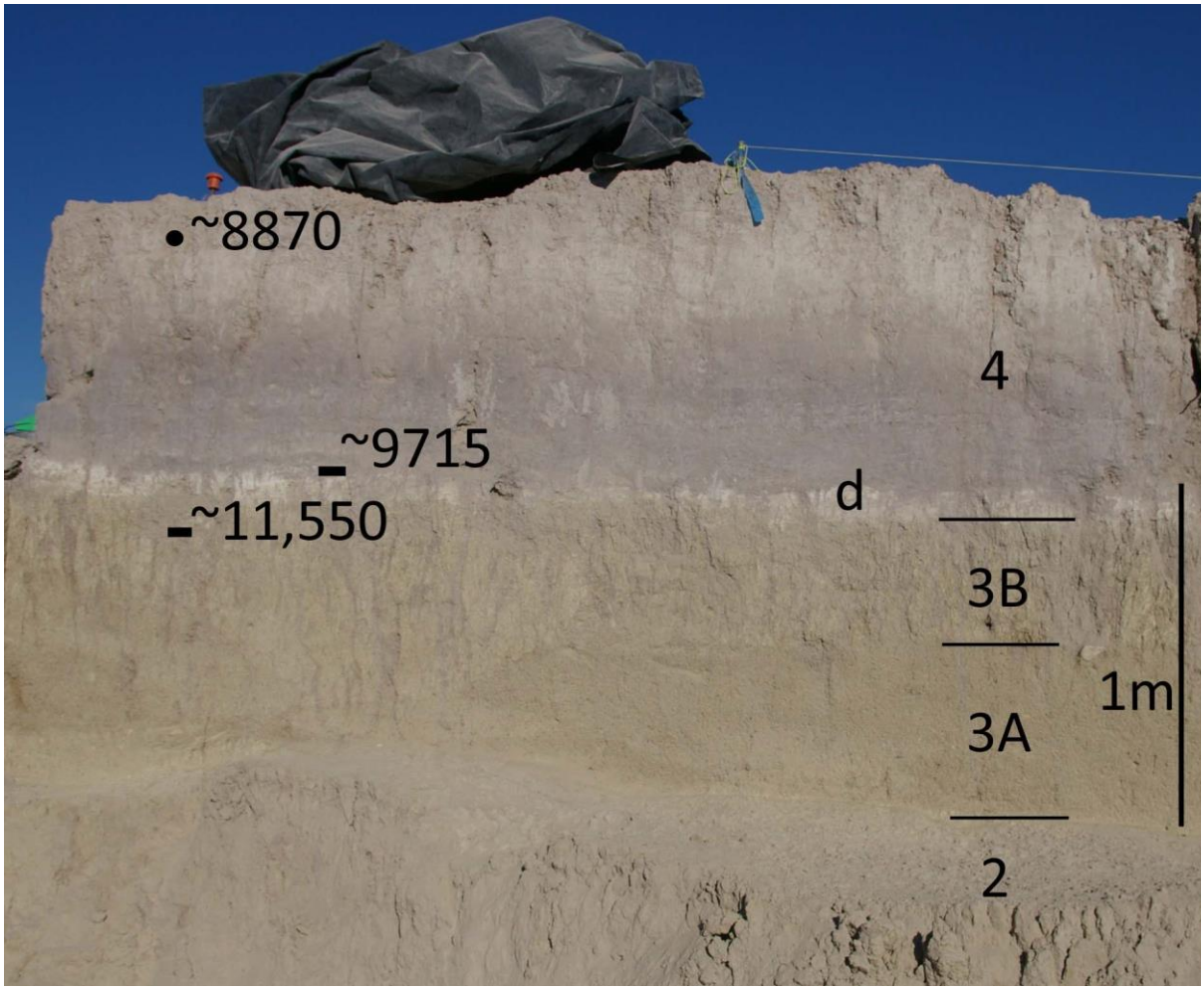

Figure S2. Stratigraphy at Locality 1 showing strata 2, 3, 4, the diatomite (d) at the base of 4, and key radiocarbon dates (C14 years) (rectangle = charcoal; circle = Succinid). Note prismatic structure in stratum 3B, formed by pervasive cracking that predates stratum 4.

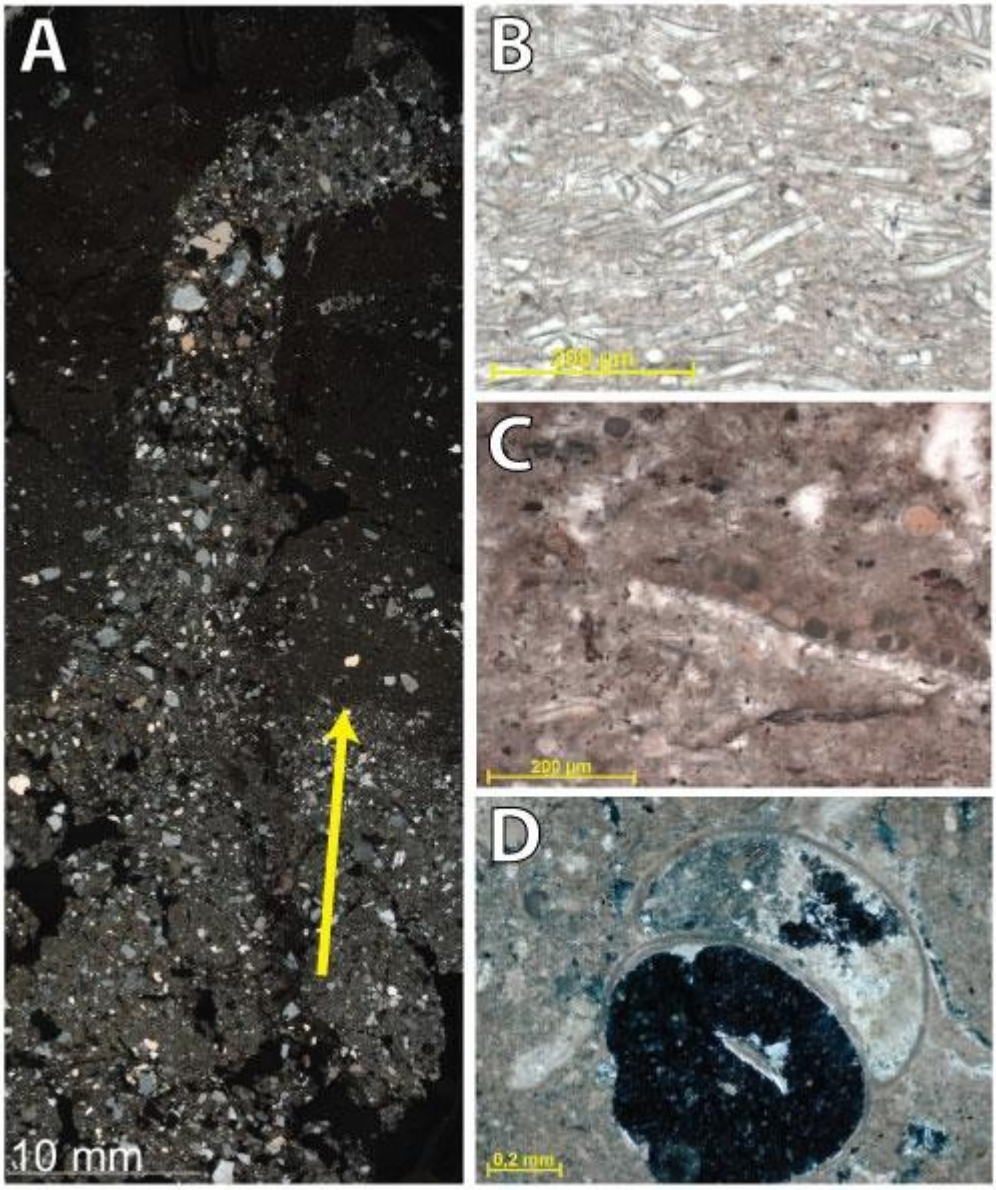

Figure S3. Microscopic characteristics of strata 3 and 4, Locality 1. A) The contact between the two strata (arrow) is abrupt and is characterized by a marked shift in composition from coarse, poorly-sorted sandy alluvium to a highly siliceous biogenic deposit containing abundant diatoms An insect burrow is present in the photomicrograph. The burrow is filled with sediment from stratum 3. Cross-polarized light, composite image. B) The base of stratum 4 contains intact diatoms with horizontal long-axis alignment. Plane polarized light. C) The middle of stratum 4 is composed of diatomaceous earth containing lenses of phytoliths (some articulated, as illustrated here) and humified organic material. Articulation of the phytoliths indicates that the plant fragments decomposed in place. Plane polarized light. D) The top of stratum 4 is calcareous and contains diatoms, phytoliths, organic material, and shell fragments. The center of the image is a cross-section through a succinid shell. The shell contains void space (black) and a calcareous infilling. Cross-polarized light.

Figure S4. Upper stratum 2 on the Locality 3 island (text Fig. 1) showing the vertical carbonate zonation (Upper Massive C1, Middle Platy C2, Lower Massive C3, Table S2) and the well-expressed Bt soil horizon ("Big Red") buried beneath the carbonate.

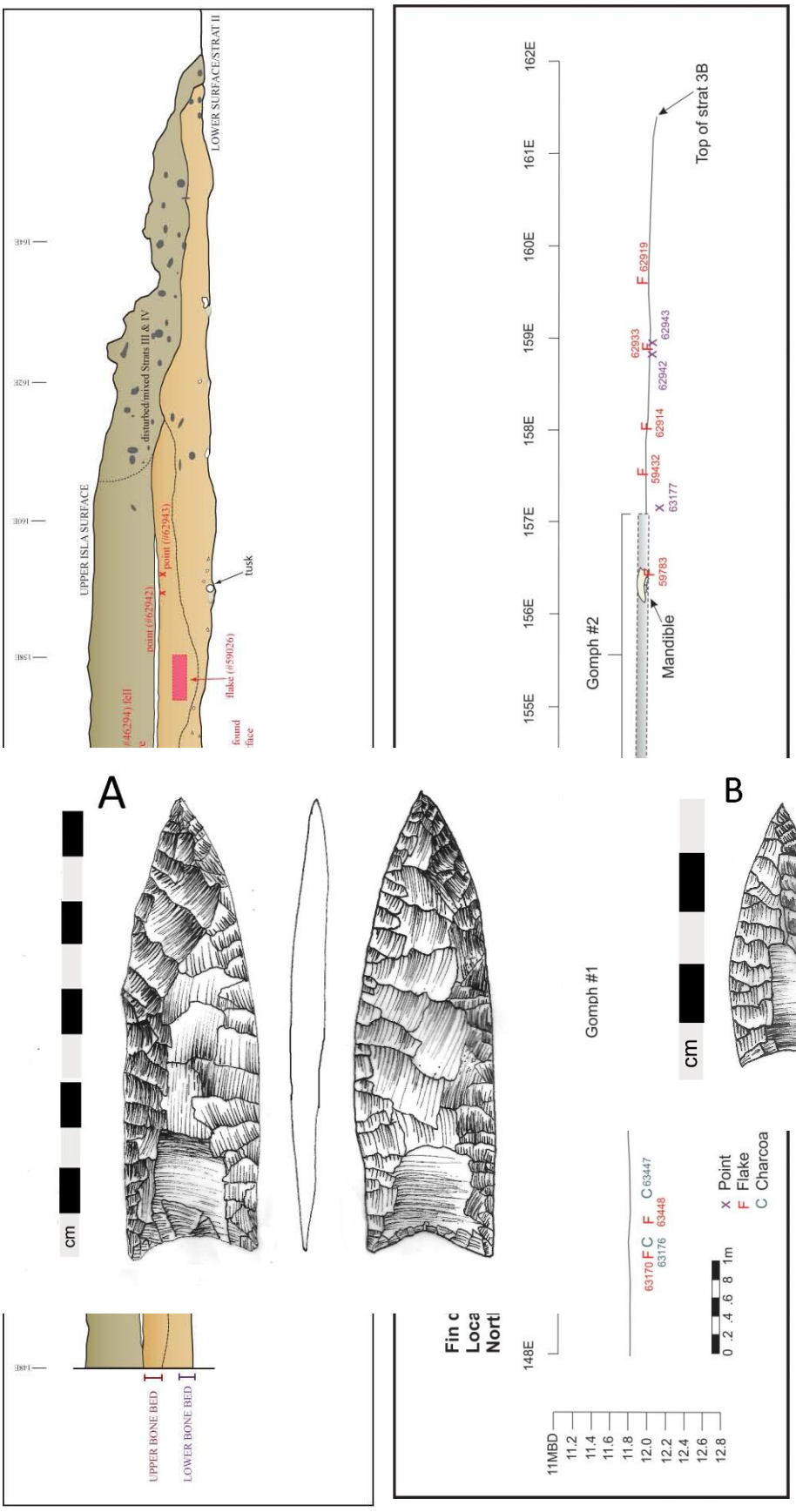

Figure S5 (left). Stratigraphy of Locality 1, south wall, before excavations

Figure S6 (right). Backplot of bone, artifacts, and charcoal along an east-west profile of locality 1, illustrating the narrow depth range of bone and stone below the top of stratum 3B.

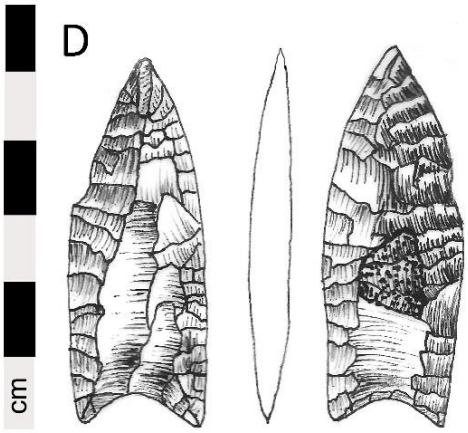

Figure S7: Projectile points found in situ in the upper bone bed at Locality 1 (A 63177; B 62943; C, C' 62942; D 63008).

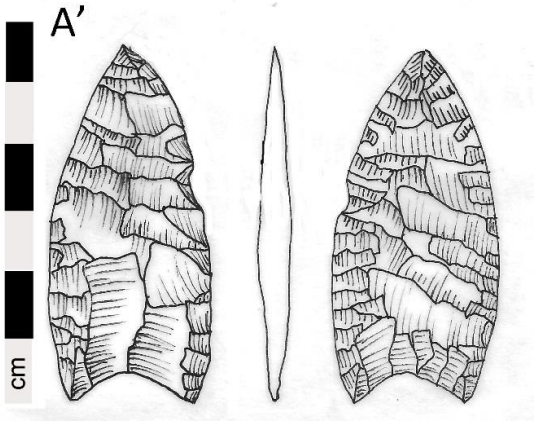

Figure S8: Clovis points from disturbed contexts in and around Locality 1 (A, A' 58342; B, B' 59569; C, C' 46023; **Next Page**).

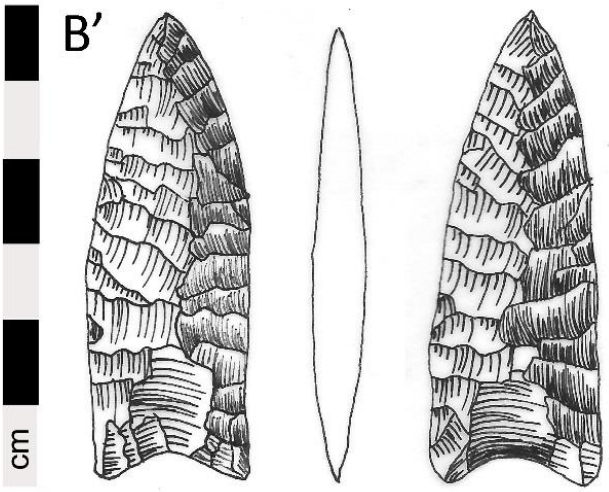


CM
C

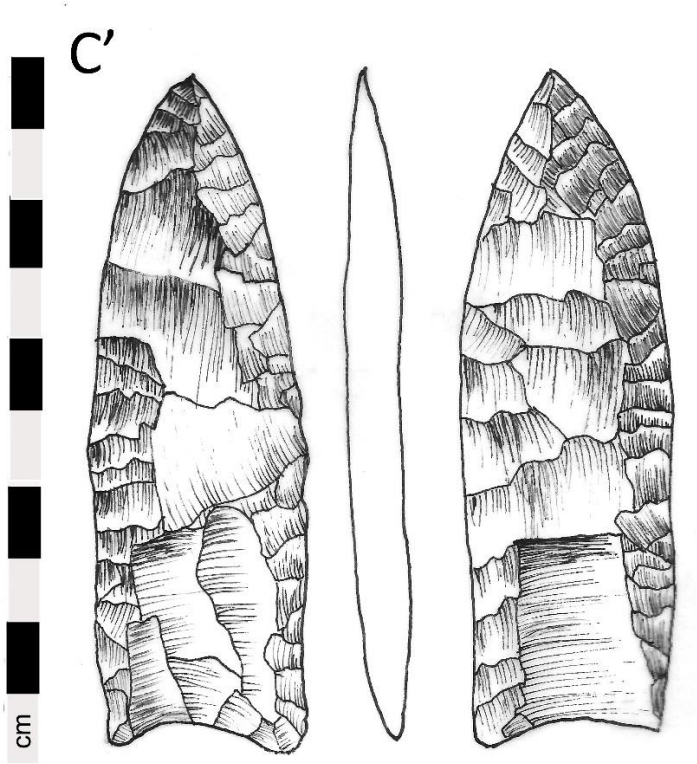
C'
cm

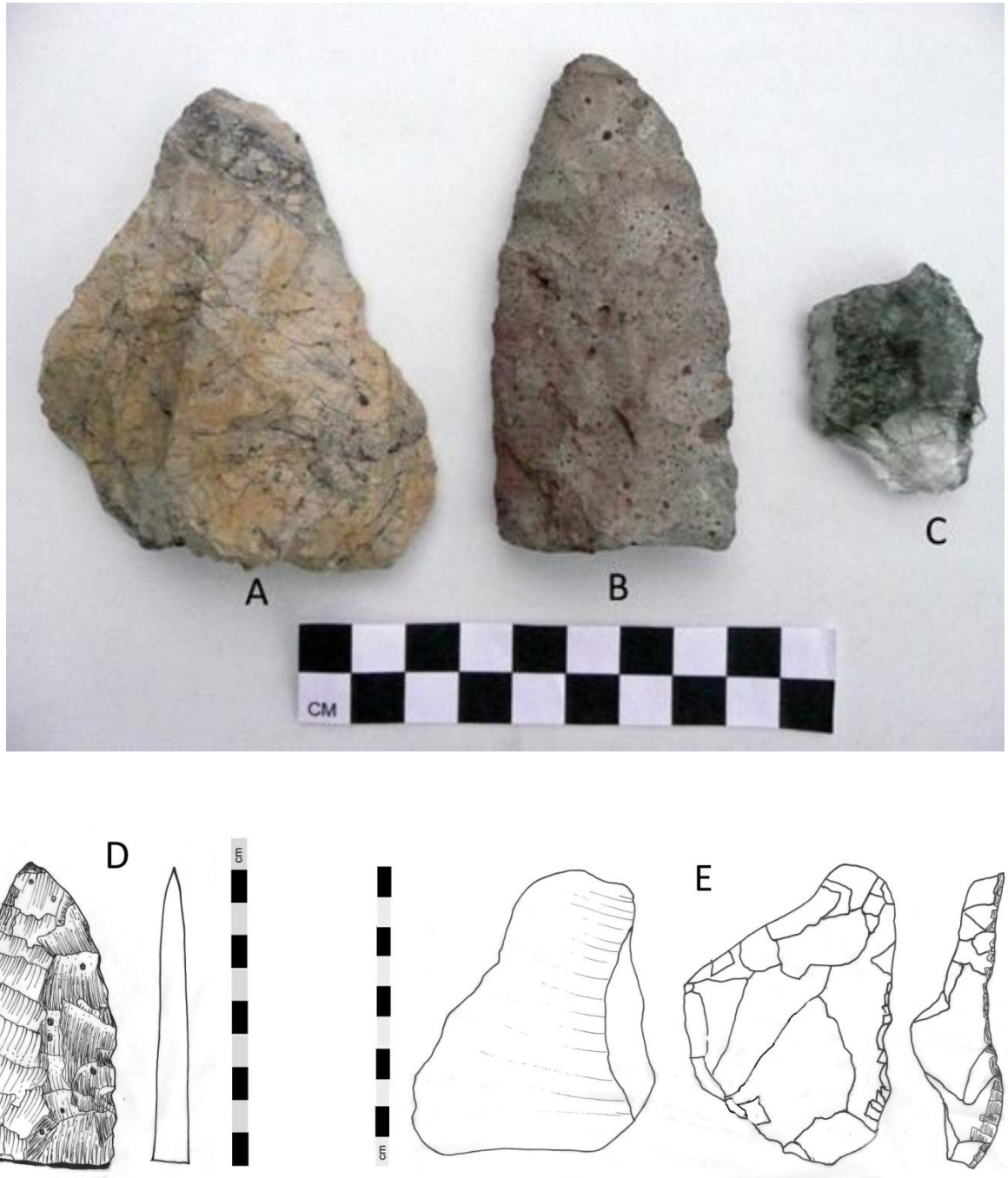

Figure S9: Artifacts from disturbed contexts around Locality 1 (A, E 45980; B, D 46021; C 46002).

Figure S10. Points 62943 (left) and 62942 (right) in place. Note the cracks in stratum 3B (formed before diatomite deposition of overlying stratum 4).

Figure S11. The south side of Locality 1 when scraper 45980 (Figs. S9A) was found (at point of trowel) directly below its impression among bone (top of red line).

Artifacts from the Surface of the Upland Camp

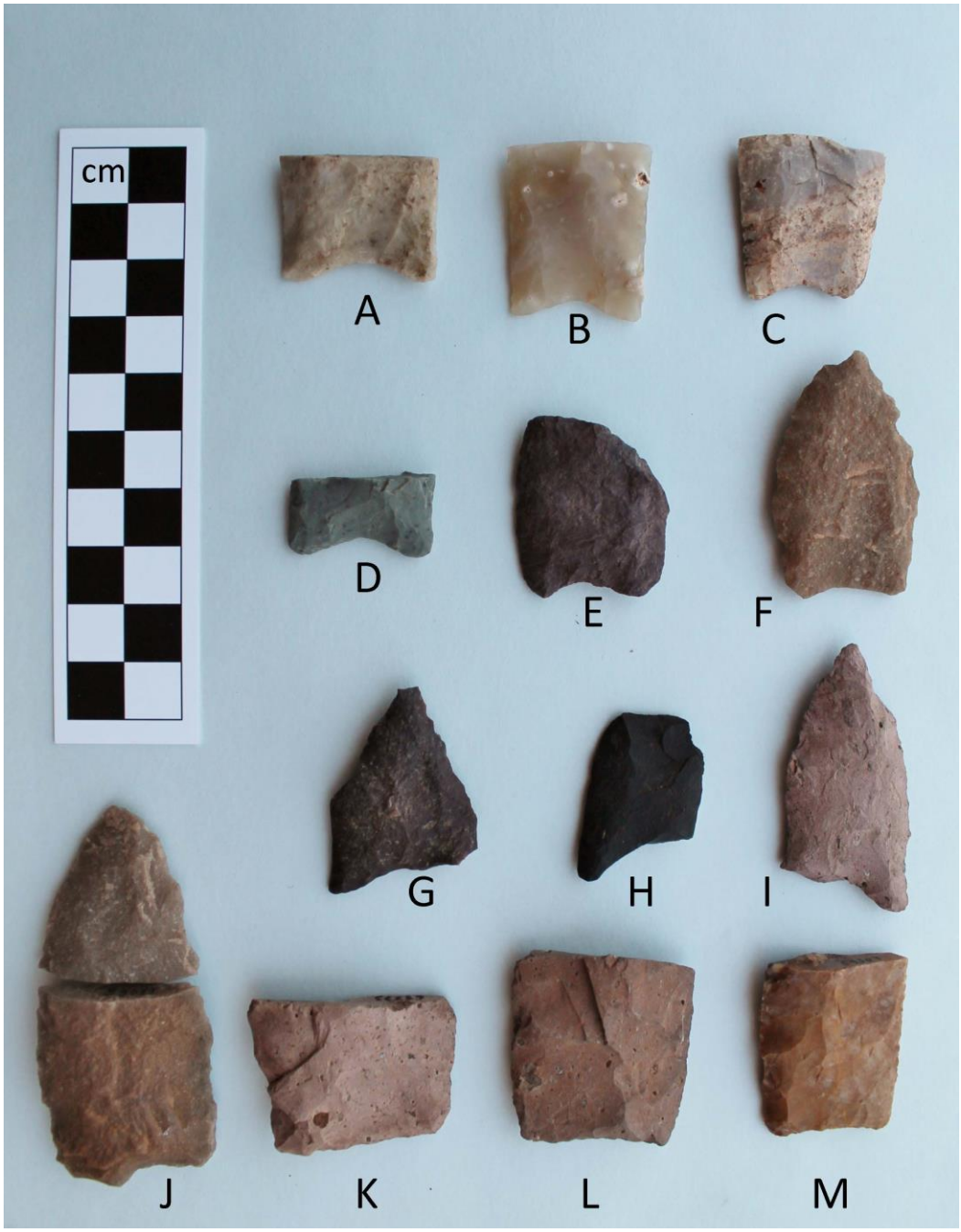

Figure S12A. Clovis projectile points and bifaces from the surface of the upland camp (A 59603; B 59593; C 59082; D 63220; E 59287; F 59332; G 59604; H 59145; I 59727; J 59083; K 63360; L 63233; M 59307).

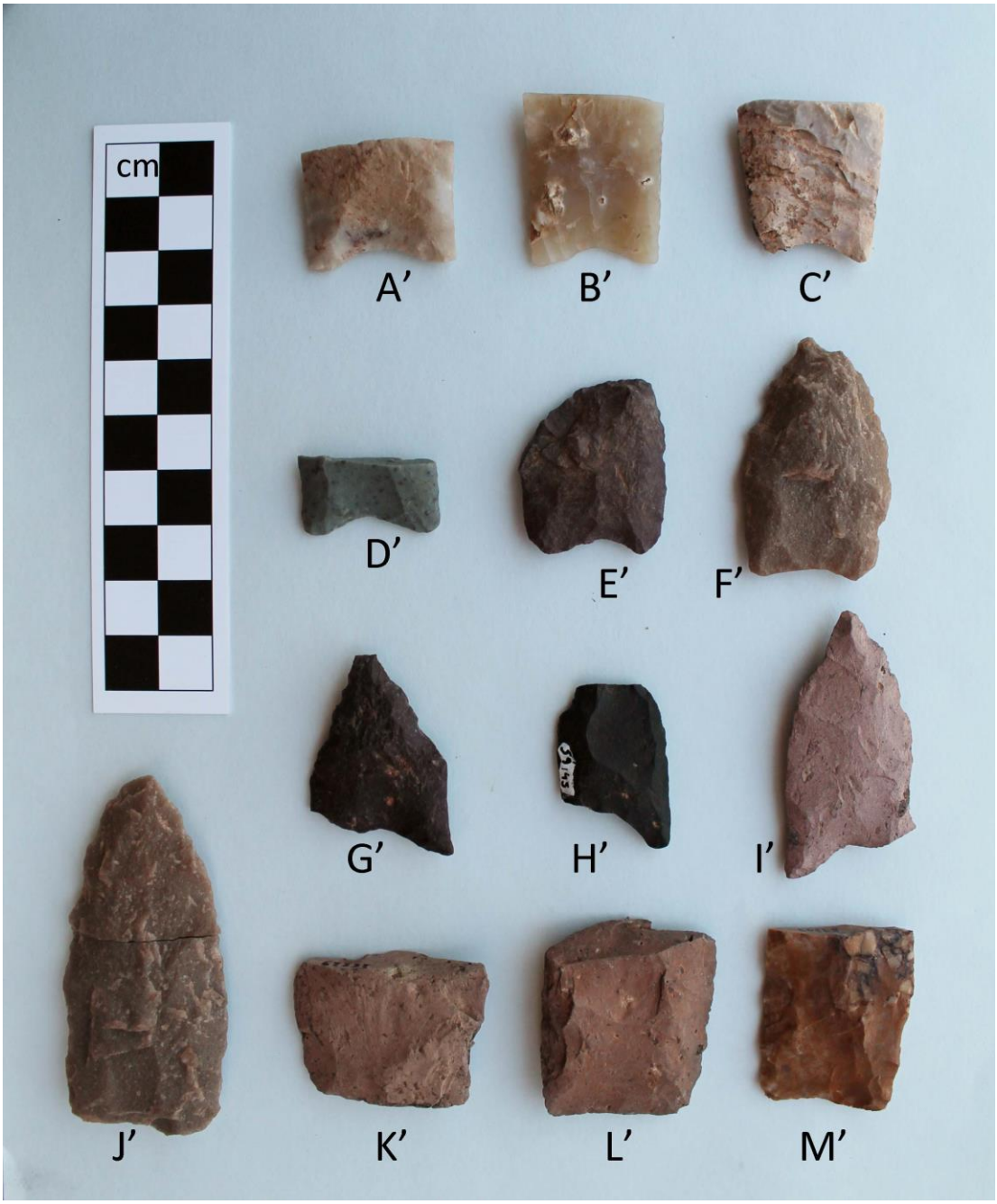

Figure S12B. Reverse side of Clovis projectile points and bifaces in Figure S12A.

Figure S13. End scrapers from the surface of the upland camp. Note the variety of raw materials.

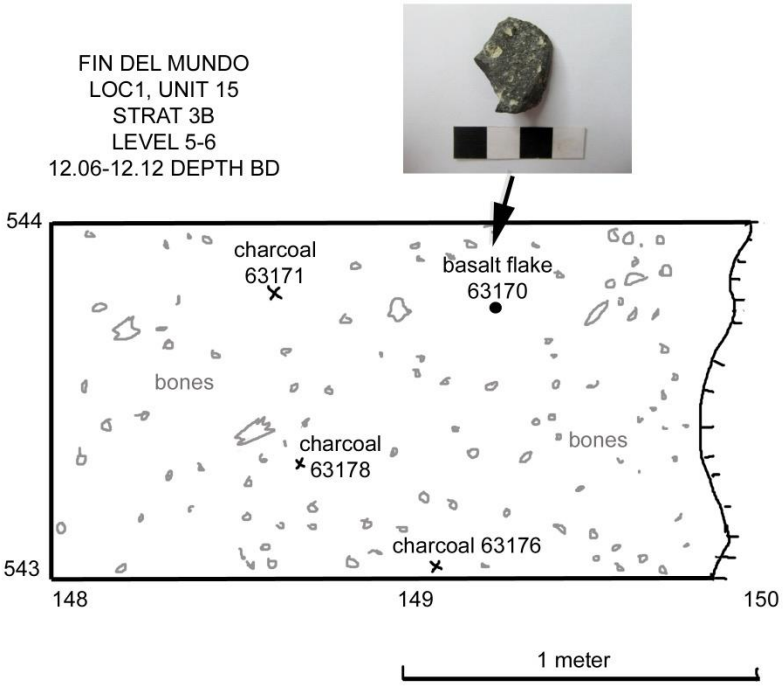

Figure S14. Unit 543N/148-150E illustrating the association of charcoal sample 63176 (^{14}C date AA100182) with a flake and bone.

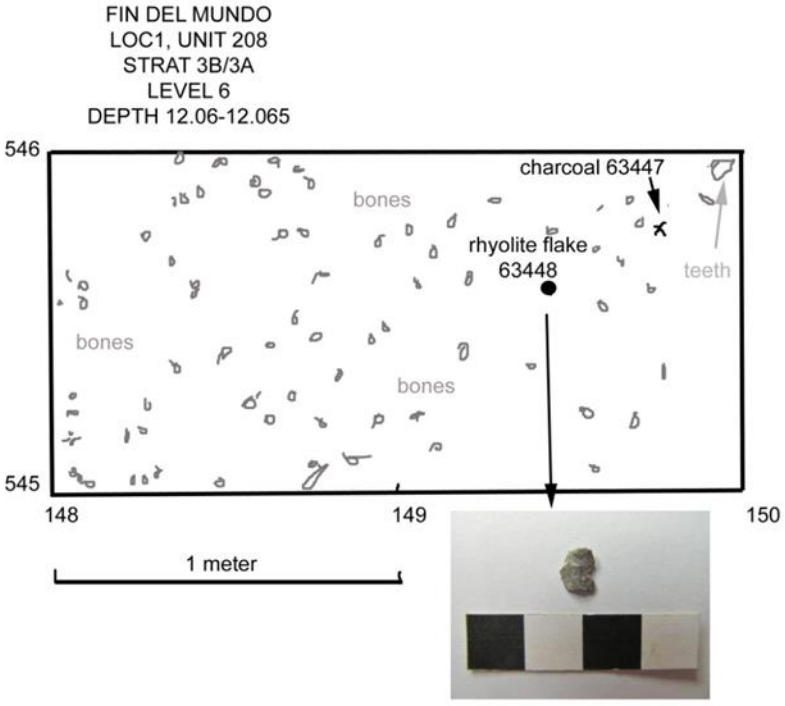

Figure S15. Unit 545N/148-150E illustrating the association of charcoal sample 63447 (^{14}C date AA100181) with a flake and bone.

Figure S16. Gomphothere M1 Right, inner enamel surface after stable isotope sampling, but before radiocarbon sampling. Distal on left.